J Mol Model (2010) 16:607–614
DOI 10.1007/s00894-009-0571-5

ORIGINAL PAPER

Probing possible egress channels for multiple ligands in human CYP3A4: A molecular modeling study

Navaneethakrishnan Krishnamoorthy · Poornima Gajendrarao · Sundarapandian Thangapandian · Yuno Lee · Keun Woo Lee

Received: 30 May 2009 / Accepted: 29 July 2009 / Published online: 29 August 2009

Abstract Human cytochrome P450 (CYP) 3A4 extensively contributes to metabolize 50% of the marketed drugs. Recently, a CYP3A4 structure with two molecules of ketoconazole (2KT) was identified. However, channels for egresses of these inhibitors are unexplored. Thus, we applied molecular dynamics simulations followed by channel analyses. Two simulations of empty and 2KT-bound CYP3A4 results revealed the multiple ligand-induced conformational changes in channel forming regions, which appear to be important for the regulation of channels. In addition, we observed that the channel-3 entrance is closed due to the large structural deviation of the key residues from Phe-cluster. F215 and F220 are known as entrance blockers of channel-2 in metyrapone-bound CYP3A4. Currently, F220 blocks the channel-3 along with F213 and F241. Therefore, it suggested that channel-1 and 2 could potentially serve as egress routes for 2KT. It is also supported by the results from MOLAxis analyses, in which the frequency of channel occurrence and bottleneck radius during simulation favor channel-1 and 2. Several bottleneck residues of these channels may have critical roles in 2KT egresses, especially S119. Our modeling study for multiple ligand-channeling of CYP3A4 could be very helpful to gain new insights into channel selectivity of CYP3A4.

Keywords Channel · Cytochrome P450 3A4 · Ketoconazole · Molecular dynamics simulation · Multiple ligands

Introduction

Cytochrome P450 (CYP) superfamily members catalyze the most important monooxygenation reaction and are thereby involved in the phase I metabolism of various endogenous and exogenous compounds including drugs and xenobiotics [1]. Historically, CYPs play a central role in drug metabolism [2, 3]. More than 90% of the drugs are metabolized by five of the most important CYP members, in which human CYP3A4 highly contributes by metabolizing 50% of the clinically used drugs [4]. To date, there are six CYP3A4 crystal structures available in protein data bank (PDB) [5–7]. It includes two ligand-free forms (1W0E and 1TQN) [5, 6] and a CYP3A4 in complex with multiple ketoconazole (CYP3A4-2KT, 2V0M). The latter one is evident for simultaneous binding of multiple ligands in CYP3A4, which displayed dramatic conformational changes upon ligand-binding [7].

The roles of channels in CYPs are very important for ligands to access and products to egress from the buried active site. Several CYP crystal structures offer details of their channels [5, 6, 8, 9]. The three reported channels of CYP3A4 are: channel-1 passes through B-C loop, channel-2 locates between β1 sheet, B-B' and F'-G' loops and channel-3 egress through the Phe-cluster (F108, F213, F215, F219, F220, F241 and F304) [5, 6]. Although crystal structures offer structural knowledge about channels, they could not provide dynamic or conformational changes in channels that might have been caused by ligand-binding [10–12]. Molecular dynamics is an alternative and very

Navaneethakrishnan Krishnamoorthy and Poornima Gajendrarao contributed equally to this work.

N. Krishnamoorthy · P. Gajendrarao · S. Thangapandian · Y. Lee · K. W. Lee (✉)
Department of Biochemistry, Division of Applied Life Science (BK21 program), Environmental Biotechnology National Core Research Center, Plant Molecular Biology and Biotechnology Research Center, Gyeongsang National University, Jinju 660-701, Korea
e-mail: kwlee@gnu.ac.kr

effective technique through which one can gather additional information regarding the ligand-induced conformational changes in channel forming regions that can open or close the channels [8, 10].

The aim of this study is to find out the possible egress channels for 2KT in CYP3A4. In order to probe the potential egress channels, molecular dynamics simulations (MDSs) and channel analyses were performed. Although steered MDS can provide elaborate perspective of product egress pathway, it shows great complexity to consider CYP3A4 with multiple ligands. Therefore, we utilized conventional MDS and MOLAxis to reveal the fundamentals of CYP3A4 channel's response to multiple ligands. Here, empty and 2KT-bound CYP3A4 simulations revealed the multiple ligand-induced conformational changes in channel forming regions, which appear to be important for the regulation of channels. The large deviation of the key residues from Phe-cluster indicates that it could enforce channel-3 to close, and thus, opens up opportunity for the available channel-1 and 2 to have more potential for 2KT egresses. Identification of channels using MOLAxis [13] further supports channel-1 and 2 also helps to uncover their key bottleneck residues.

Materials and methods

Modeling of missing regions and energy minimization

Crystal structures of human CYP3A4 in complex with 2KT (PDB ID: 2V0M) [7] and ligand-free form (PDB ID: 1TQN) [6] were obtained from PDB (http://www.rcsb.org/pdb/). It was noticed that the 2V0M structure has missing G-H (T264-R268) and H-I (N280-K288) loops along with its regular missing of a few of the N- and C-terminal residues. 1TQN also has missing H-I loop (K282-E285). These missing loops were modeled by employing protein modeling within Discovery Studio (DS) V2.0 [14]. Resulting structures were energy minimized using GROMACS V3.3 [15] by applying steepest descent algorithm with a tolerance of 2000 kJ mol^{-1} nm^{-1}. PRODRG web server was used to construct the ligands topology [16].

MDSs for the empty and the 2KT-bound CYP3A4

The GROMOS96 force field was applied for MDSs [17]. The structures were solvated in a cubic water box (1.2 nm) with SPC3 [18] water model and periodic boundary conditions were applied in all directions. All bonds were constrained using LINCS algorithm [19] and SETTLE [20] algorithm was used for the water molecules. A twin range cutoff was used for long-range interactions: 0.9 nm for van der Waals and 1.4 nm for electrostatic interactions. In order to neutralize the system, 4 water molecules were replaced by Cl ions. In total, CYP3A4 and CYP3A4–2KT comprised of 86045 and 86137 atoms, respectively. To equilibrate each system, 100 ps MDS was performed with position restraints. Equilibrated systems were further subjected to 5 ns production MDSs with a time step of 2 fs at constant pressure (1 atm), temperature (300 K), and number of particles. The snapshots were collected at every 5 ps for further analyses. Geometrical properties of protein and channel distances were analyzed employing tools integrated with GROMACS.

Analyses for the identification of possible egress channels

MOLAxis is well-known for its accurate identification of existing biologically relevant channels in macromolecules. MDS snapshots at every 500 ps were considered to probe the existence of possible egress channels for 2KT in CYP3A4 using MOLAxis web server. If a channel was consistently found in collected frames and coincides with the previously reported channel in CYPs then it was considered as one of the possible egress channels for 2KT. Moreover, channel which comprises bottleneck radius greater than 0.12 nm was considered relevant for ligand egress [9]. In the channel analyses, all the hydrogen atoms were included. MOLAxis was allowed to find a high success rate source point in the center of the main void. The heme molecule was included as heteroatom. The other MOLAxis parameters used for this study are: i) resolution 0.5 Å, ii) channels that split from main channel after 4 Å are neglected, iii) 30 Å bounding sphere radius, and iv) sphere display limited to 4 Å. The interactive visualization program Chimera was used to represent channels.

Results and discussion

Multiple ligand-induced conformational changes in channel-forming regions

In order to provide access or egress pathway for ligands the protein's dynamic motions can be essential [10–12]. Furthermore, several CYPs underwent conformational changes upon ligand-binding [21–23], which were also illustrated in the CYP3A4–2KT crystal structure [7]. To that extent, we believe that the conformational changes by multiple ligand-binding may be essential for the ligand-channeling in CYP3A4. Therefore, to investigate the ligand-induced conformational changes especially in the channel forming regions, geometric properties of CYP3A4 with and without 2KT were analyzed throughout the MDS.

The root-mean-square deviation (RMSD) of the protein was measured with respect to the initial structure as a

function of time for the protein Cα-atoms (Fig. 1a). The plot for the CYP3A4-2KT gradually increased till 0.17 nm and remained with slight fluctuation for the rest of the MDS, which indicates that the structure is relatively stable during MDS. In contrast, RMSD for the 2KT-free form reached 0.25 nm at 2 ns and maintained till the end of the MDS. These results suggest that the structural deviations of CYP3A4 depend upon multiple ligand-binding.

The average root-mean-square fluctuation (RMSF) results demonstrated the highly flexible and stable regions of CYP3A4 during MDSs (Fig. 1b). In both systems, the plastic regions were found to be flexible, including key channel forming regions B-C loop and F-G (including helices F, F', G, G') region. In general, B-C loop, helices F-G and their connecting loops were reported as flexible regions of CYPs [24]. The dynamic motions of these helices were proved to be involved in opening/closing of channels thereby helps for ligand entry/exit [25]. The overall RMSF comparison of two systems denoted that the plastic regions and a few core regions were relatively more flexible in the free form than the 2KT-bound CYP3A4. High fluctuation of the constructed missing loops, G-H and H-I evidently indicates why these regions were missing in the crystal structure data. However, the rest of the protein core regions were stable in the free and ligand-bound forms. These RMSF results elucidate the flexible and stable regions of the protein upon multiple ligand-binding.

To represent the detailed deviation of each structural element between two forms of CYP3A4, the lowest energy structures from both the MDSs were selected and their Cα-atoms were superposed (Fig. 1c). This superimposition yields overall protein deviation of 0.24 nm, which was higher than the observed 0.18 nm by X-ray structures overlay [7]. Superimposition of channel forming structural elements (region by region) further exhibited the most predominant conformational changes in B-C loop and F-G region that deviated 0.34 nm and 0.37 nm, respectively. Helix I (0.15 nm) and β1 sheet (0.13 nm) are the other channel forming regions, which also displayed minor deviations. It is interesting that significant motion were found in channel neighboring regions, helices B, C, G and H, and a few β-sheets. Altogether, results of our MDS analyses evidently demonstrate the deviations of many structural elements, which are induced by multiple ligand-binding in CYP3A4. These prominent conformational changes in channel forming and their neighboring regions upon ligand-binding indicate that they could be inevitable for the regulation of channels for 2KT in CYP3A4.

The significant protein-ligand interactions that anchor the ligands inside the active site of CYP3A4 were monitored in the course of MDS (Figs. 1d and e). The KT1 is located above the heme (near channel-1) and bound to the Fe by its imidazole nitrogen atom [7]. The distance between the Fe and the nitrogen atom was stable all over the MDS to keep the ligand in place along with

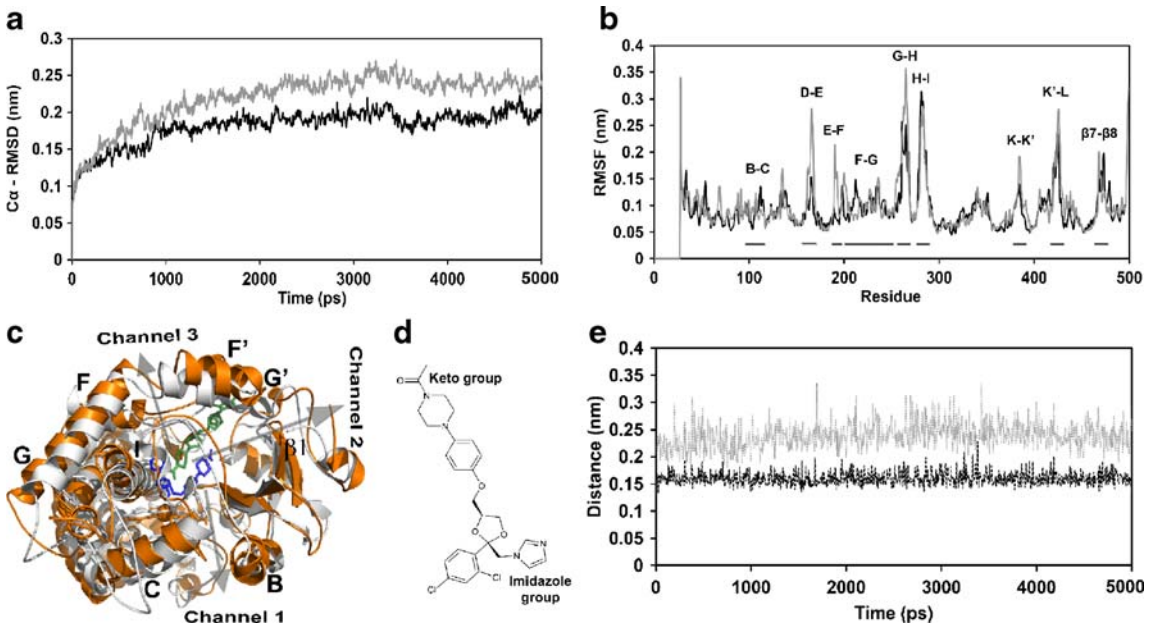

Fig. 1 Multiple ligand-induced conformational changes in channel forming regions and key interactions. (**a**) RMSD and (**b**) RMSF of 2KT-free and 2KT-bound CYP3A4 are represented in gray and black lines, respectively. (**c**) Superimposed lowest energy structures of free (white) and ligand-bound CYP3A4 (orange), in which arrows represent channels, heme and KT1 shown as blue sticks, and KT2 as green sticks. (**d**) 2D illustration of ketoconazole. (**e**) Distance between the nitrogen atom of KT1 imidazole group and the Fe of heme drawn as gray dotted line and distance between the oxygen atom of KT2 keto group and S119 depicted in black dotted line

the other interacting residues (F57, R106, I120, L211, M371, I300, I301, and L482). The oxygen atom of the keto group in the KT2 forms hydrogen bond with S119 and the imidazole group of KT2 is located near the channel-2. This hydrogen bond was highly conserved all over the MDS and it anchored the ligand together with the other active site residues (R106, I120, L211, F213, F215, F220, and L221). A highly conserved S119 is found to be a key determinant of CYP3A4 specificity, which is involved in substrate binding or recognition [26, 27]. This finding is consistent with the role of S119 observed from our study. We suspect that these ligand-protein interactions are crucial for egresses of 2KT from the CYP3A4 active site.

Distances between the key residues of channels

The channels that are not viewed in the crystal structure could be opened by dynamic motions [11, 12]. A recent conventional MDS study of CYP3A4 exhibited possible channels for metyropone egress [28]. In order to predict possible egress channels for 2KT in CYP3A4, the distance between center of mass of channel key residues were measured in the course of MDS for empty and 2KT-bound forms. The six pairs of key residues, which are residing on opposite sides of each channel were considered for this calculation: P107↔I120 and F108↔S119 in channel-1, N79↔P107 and N79↔T224 in channel-2, and F213↔F241 and F213↔F304 in channel-3.

There was no major change in the distance between channel key residues of 2KT-free CYP3A4 over the MDS (Fig. 2a). Likewise, in CYP3A4-2KT, channel-1 and 2 maintained their initial distances (Fig. 2Ba and 2Bb). The distance analyses results indicate that these channels could be available for ligand egress in CYP3A4–2KT (in free form for entry/egress). Conversely, channel-3 distance (F213↔F241) of CYP3A4–2KT decreased from 1.1 nm to 0.8 nm and remained (after 800 ps) until the end of MDS (Fig. 2Bc). This significant decrease in the distance indicates that channel-3 possibly approaches to its closing state. This finding disagrees with the results of the other modeling study of CYP3A4-metyrapone complex, where channel-2 closed during conventional MDS [28]. A site directed mutagenesis study of CYP2B1 also uncovered a similar result [29]. However, few reports have revealed that CYPs probably provide channels depending upon their ligands [8, 9, 12]. To that extent, our results indicate that this protein may provide available channel-1 and/or 2 for 2KT egresses.

Although the distances of these channels appear to be similar (0.8 nm), the decreasing trend of channel-3 from its initial structure was mainly taken into account. This is very similar to the results of the previous MDS study of CYP3A4-metyrapone complex (closed channel-2 (0.8 to 0.6 nm) and possible open channel-3 (maintained between 0.6–0.7 nm)) [28]. In this study, the largest distance (1.4 nm) was observed between the key residues (F213↔F304) that are located at the inner end of the

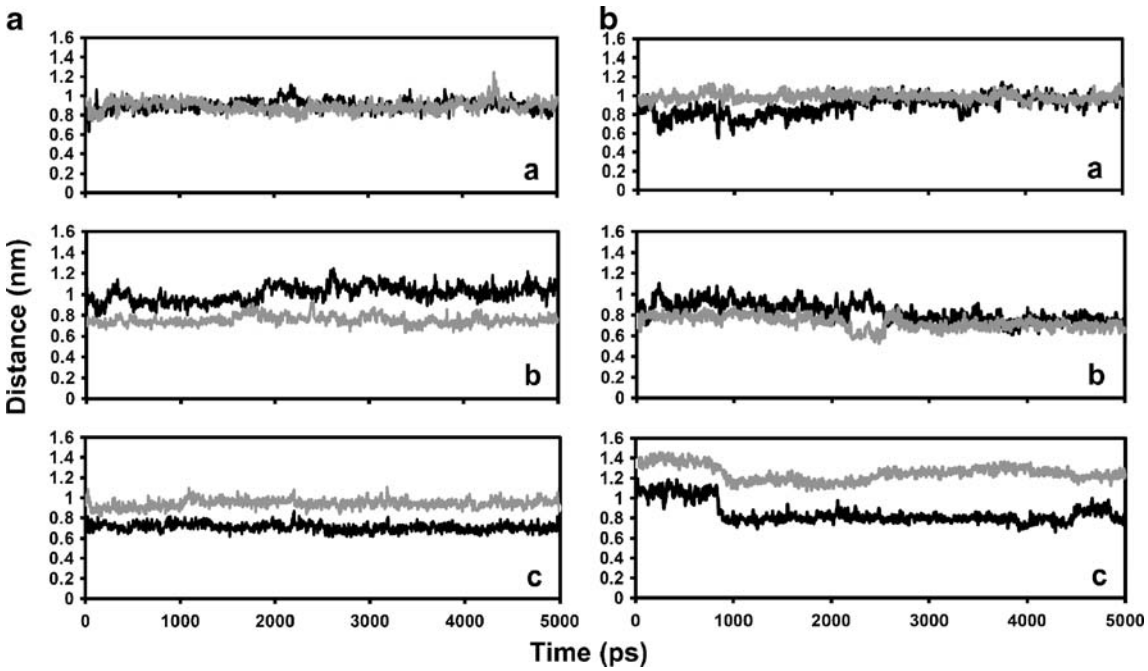

Fig. 2 Distances between the key residues in channels. (**A**) Distances of 2KT-free form channels. (**B**) Distances of 2KT-bound CYP3A4 channels. (**a**) Channel-1, (**b**) Channel-2 and (**c**) Channel-3 where, distance between residues P107↔I120, N79↔P107, and F213↔F241 are represented in black lines and gray lines denote the distance between residues F108↔S119, N79↔T224 and F213↔F304

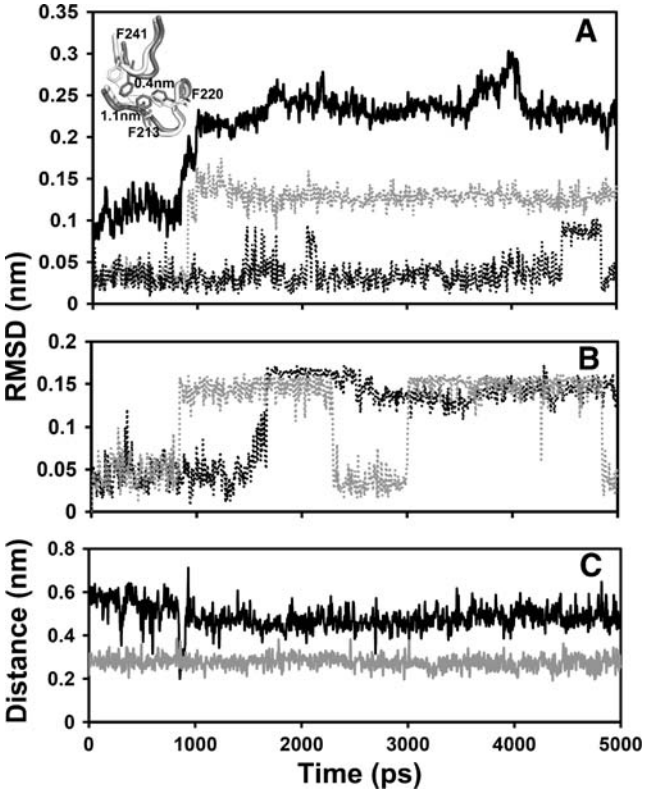

Fig. 3 Structural deviations of the key elements in channel-3. (**a**) RMSD plot of highly deviated Phe-cluster and channel-3 bottleneck residues F213 and F241 are depicted in black, dotted gray and dotted black lines, respectively. Cartoon inside the plot area shows superposition of the F'-G' loop structures, which have large (white) and small (gray) bottleneck distance during MDS. The key residues are drawn as sticks. (**b**) F215 and F220 deviations are plotted in gray and black dotted lines, respectively. (**c**) Distance between side chains of F220 and F213 and F220 and F241 are plotted using gray and black lines, respectively

channel-3. Although the inner end of channel-3 appears to be available during the simulation, the distance between the key residues (F213↔F241) at the other end of channel-3 was decreasing, which indicate that this channel may not be available for ligand egress. It is proved that the ligand egress required high rupture force and significant conformational change in order to open channel-3 [28], which is also not favorable for ligand egress through channel-3 in our study.

Channel-3 runs through the signature Phe-cluster of CYP3A4 (between F-F', G-G' loops and I helix). Most of the Phe-cluster residues are located at F-G region except F108 and F304. The structural deviation of Phe-cluster residues with respect to their initial position was analyzed to identify the key elements responsible for channel-3 gating. The deviation of the key residues F213 and F241 indicates their significance in channel-3 gating by side chain motion (Fig. 3a). The channel-3 structures with the highest (20 ps) and the lowest (4290 ps) bottleneck distances were examined. The result showed that the distance between F213 and F241 side chains decreased from 1.1 nm to 0.4 nm. In addition, the overall deviation of Phe-cluster (Fig. 3a) has increased during MDS, especially due to the fluctuation of F213, F215, F220, and F241 (Figs. 3a and b). The distance between F220 and channel bottleneck residues (F213 and F241) illustrated that this residue remained in close proximity to the channel-3 entrance to block the ligands (Fig. 3c). These findings indicate the importance of Phe-cluster in the regulation of channel-3 of CYP3A4-2KT. In the CYP101 F-G region, small backbone motion (2 Å) and fluctuation of the aromatic residues appeared to act as a selectivity filter for ligands [9, 10]. The closing of channel-2 in CYP3A4-metyropone complex was monitored during conventional MDS, which occurred due to the shift of channel-2 forming structural elements including F'-G' region and F215 and F220 rearrangement [28]. In sum, it indicates that the residue F220 is not only involved in the closing of channel-2 but also may play a major role in closing the entrance of channel-3 with other gating residues of the Phe-cluster. These results suggest that the residues F213 and F241 together with F220 block the channel-3 instead channel-2 in CYP3A4-2KT.

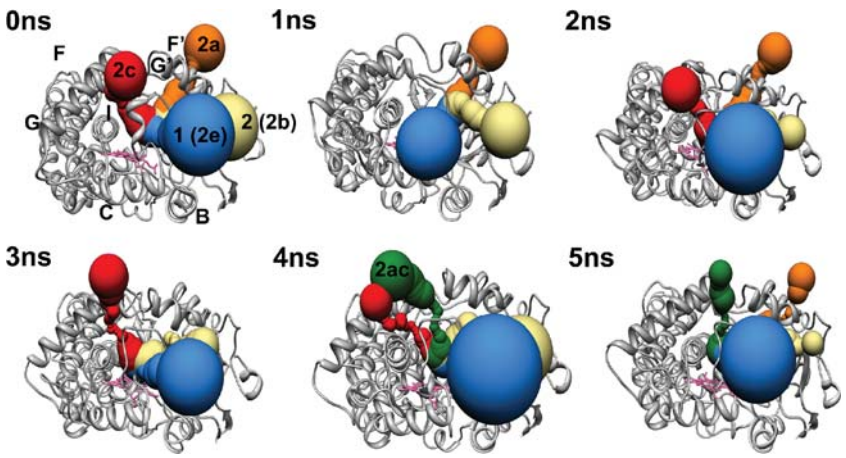

Fig. 4 Possible CYP3A4 channels for 2KT egresses. The identified biologically relevant channels for possible egress at every 1 ns of 5 ns MDS are depicted as color spheres: channel-1 (**2e**); blue, channel-2 (**2b**); khaki, **2a**; orange, **2c**; red and **2ac**; green

Table 1 The possible egress channels for 2KT in CYP3A4 identified by MOLAxis from MDS snapshots

Channel	Frequency of occurrence in simulation											Bottleneck residues	
	Time (ns)											Most repeated	2nd most repeated
	0	0.5	1	1.5	2	2.5	3	3.5	4	4.5	5		
1 (2e)	1	1	1	1	1	1	1	1	1	1	1	R105, R106, S119, I120	F108
2 (2b)	1	1	1	1	1	1	1	1	1	1	1	R106, P107	Q79
2a	1	1	1	1	1	-	-	1	-	1	1	L216, L221	I50
2c	1	1	-	1	1	1	1	1	1	-	-	F113	L293, V296
2ac	-	-	-	1	-	-	-	-	1	-	1	-	V111, F241

Identification of the possible egress channels for 2KT in CYP3A4

In most CYPs, channel-2 subclasses are lined by B-C/B-B' loop, in which channel-2e and 2b are similar to channel-1 and 2 of CYP3A4, respectively [9, 13, 28]. Since channel-3 has demonstrated its possible closing in MDS, we suspect either channel-1 or 2 could be the potential candidates to provide egress path for 2KT. In order to confirm the potential egress channels, the frequency of channel occurrence was analyzed for every 0.5 ns snapshots of MDS using MOLAxis. The bottleneck radius of channels was also considered, because it indicates the potential openings for ligand entry or egress [9, 13]. Figure 4 and Table 1 illustrate the existence of biologically relevant channels during MDS. Channel-1 was frequently identified in all collected snapshots, whose average bottleneck radius was 0.16 nm (Table 2). In this channel, the residues R105, R106, S119, and I120 were found to be involved most repeatedly in the bottleneck construction. Moreover, channel-2 was also detected in every 0.5 ns snapshots. Average bottleneck radius of this channel was 0.18 nm, which was slightly higher than channel-1. In the construction of channel-2 bottleneck, P107 was a frequent contributor. Channels 2a and 2c have also been identified in most of the collected snapshots, in which 2a egress in the vicinity of the F'-G' loop and 2c runs through G, I helices and B-C loop. A comparison of average bottleneck radii of 2a (0.13 nm) and 2c (0.09 nm) suggests that 2a has a greater possibility to be an egress channel than 2c. L216 and L221 were often involved in the bottleneck formation of channel-2a.

Channel-3 was not obtained with reasonable ranking by MOLAxis, thus it was not considered as a potential egress channel even in the initial phase of MDS. We believe that this might be due to the intrusion of the residues that form subclasses of channel-2 (2a and 2c, neighbors of channel-3). According to the frequency of channel occurrence, average bottleneck radius and the position of ligands (Fig. 1c), we speculate that channel-1 and 2 could be the most possible egress channel providers for KT1 and KT2, respectively. Nevertheless, there may be a possibility for both ligands to egress through the same channel (1 or 2). Although channel-2a and 2c have high frequency of occurrence (located near ligands), yet the bottleneck radii of these channels have been decreased over the MDS. Therefore, they have very low possibility to serve as egress routes for 2KT.

S119 play a key role in CYP3A4 ligand-specificity [26, 27]. In addition to the preserved hydrogen bond between S119 and the ligand (Fig. 1e), channel analyses revealed this S119 as a bottleneck residue (Table 1). These results indicate that this residue could play significant role in multiple ligand-channeling of CYP3A4. Most of the identified bottleneck residues from MOLAxis analyses are compatible with the key residues that are used for distance analysis of channels, which could be critical for the

Table 2 Bottleneck radius for the identified channels of CYP3A4

Channel	Bottleneck radius (BR) (nm)											Average BR (nm)
	0ns	0.5ns	1ns	1.5	2ns	2.5	3ns	3.5ns	4ns	4.5	5ns	
1 (2e)	0.16	0.14	0.12	0.16	0.16	0.15	0.18	0.15	0.15	0.21	0.16	0.16
2 (2b)	0.13	0.23	0.2	0.17	0.22	0.2	0.11	0.14	0.21	0.2	0.13	0.18
2a	0.13	0.16	0.16	0.15	0.17	-	-	0.09	-	0.1	0.07	0.13
2c	0.12	0.11	-	0.06	0.12	0.09	0.09	0.08	0.08	-	-	0.09
2ac	-	-	-	0.07	-	-	-	-	0.09	-	0.08	0.08

regulation of channels in CYP3A4–2KT. Moreover, our channel analyses suggest that the residues A105, A106, F113, L216, and L221 are also important for the egresses of 2KT.

Biologically relevant egress channels for 2KT

MDS studies of several CYPs [8, 9, 11, 30] and X-ray structure study of CYP51 [31] supported the channel-1 to be a potential passage for ligands. In particular, a recent modeling study of CYP3A4 proposed that channel-1 can serve as an egress route for the inhibitor, metyropone [28]. Therefore, this channel-1 appears to be one of the most possible egress channels for another CYP3A4 inhibitor ketoconazole. In bacterial CYPs, 101 [32] and 102 [33] have a channel between F-G loop and β1 sheet that is similar to channel-2 in CYP3A4. MDSs of these bacterial CYPs elucidated that they could allow ligands to pass through this channel by shifting B-C loop away from F-G loop. This channel-2 was also detected as a secondary egress route provider for products in few mammalian CYPs [9]. While considering these findings we speculate that the channel-2 in CYP3A4 might serve as another egress channel for multiple ligands. The observed subclasses of channel-2 in CYP3A4–2KT (2b, 2a, 2c and 2ac) are commonly identified in other CYPs. In particular, various MDSs and experimental data signify the ability of channels 2a and 2c to open up for ligand egress [10–12]. The merging of these sub channels was also frequently noticed [9]. Our results for channel-3 along with the finding of closed channel-2 from the CYP3A4-metyropone study suggest that the key Phe-cluster residue F220 appears to be vital for both channel-2 and 3 gating. However, anyone can be blocked at a time. Here, it is channel-3.

Although available channels for 2KT in CYP3A4 shows maximum bottleneck radius of 0.21 nm or 0.23 nm (Table 2), deviations of channel structural elements could be the key to open up the channel further for egress when the ligands approach their entrances. Furthermore, all the above channels are depended on the highly flexible B-C and F-G loops [9]. Our MDS results illustrated that the structural deviation of Phe-cluster (F-G loop) closed channel-3. It also revealed the deviation of other channel forming regions (B-C loop), which could help 2KT egresses through channel-1 and 2. Therefore, the conformational changes of these loops can determine the proper egress channels for multiple ligands.

Conclusions

Our molecular modeling study suggests that channel-1 and 2 of CYP3A4 could serve as possible egress channels for 2KT. Additionally, the other subclasses of channel-2 (2a and 2c) might have very low possibilities. Several bottleneck residues are expected to play key roles in 2KT egresses from the active site. However, channel-3 may not be a potential egress route for both inhibitors due to the gating of three Phe-cluster residues. This indicates that CYP3A4 may use channel-1 for egress (single or multiple ligands) as it used for metyrapone egress [24]. Conversely, it shows different behavior by closing channel-3 (channel-2 in CYP3A4-metyrapone) and leaving channel-2 as another possibility for multiple ligands egresses. These findings have led us to propose that this protein can provide different egress channels for multiple ligands. The current study has important implications for understanding the channel selectivity of CYP3A4 for multiple ligands.

Acknowledgments The authors express their great gratitude to the reviewers for their valuable suggestions. N. Krishnamoorthy, P. Gajendrarao, S. Thangapandian and Y. Lee were supported by scholarship from the BrainKorea21 program, Ministry of Education, Science and Technology, Korea and this work was supported by grants from MOST/KOSEF for Environmental Biotechnology National Core Research Center (grant #:R15–2003–012–02001–0).

References

1. Guengerich FP (1994) Toxicol Lett 70:133–138
2. Guengerich FP (2008) Chem Res Toxicol 21:70–83
3. Lamb DC, Waterman MR, Kelly SL, Guengerich FP (2007) Curr Opin Biotechnol 18:504–512
4. Williams JA, Hyland R, Jones BC, Smith DA, Hurst S, Goosen TC, Peterkin V, Koup JR, Ball SE (2004) Drug Metab Dispos 32:1201–1208
5. Williams PA, Cosme J, Vinkovic DM, Ward A, Angove HC, Day PJ, Vonrhein C, Tickle IJ, Jhoti H (2004) Science 305:683–686
6. Yano JK, Wester MR, Schoch GA, Griffin KJ, Stout CD, Johnson EF (2004) J Biol Chem 279:38091–38094
7. Ekroos M, Sjogren T (2006) Proc Natl Acad Sci USA 103:13682–13687
8. Wade RC, Winn PJ, Schlichting I, Sudarko (2004) J Inorg Biochem 98:1175–1182
9. Cojocaru V, Winn PJ, Wade RC (2007) Biochim Biophys Acta 1770:390–401
10. Ludemann SK, Lounnas V, Wade RC (2000) J Mol Biol 303:797–811
11. Winn PJ, Ludemann SK, Gauges R, Lounnas V, Wade RC (2002) Proc Natl Acad Sci USA 99:5361–5366
12. Schleinkofer K, Sudarko WPJ, Ludemann SK, Wade RC (2005) EMBO Rep 6:584–589
13. Yaffe E, Fishelovitch D, Wolfson HJ, Halperin D, Nussinov R (2008) Proteins 73:72–86
14. Discovery Studio 2.0 User Guide (2005) Accelrys Inc, San Diego, CA, USA
15. Spoel DV, Lindahl E, Hess B, Groenhof G, Mark AE, Berendsen HJC (2005) J Comp Chem 26:1701–1718
16. Schuettelkopf AW, van Aalten DMF (2004) Acta Crystallogr D 60:1355–1363
17. Van Gunsteren WF, Billeter SR, Eising AA, Hunenberger PH, Kuger P, Mark AE, Scott WRP, Tironi IG (1996) The GROMOS96 manual and user guide. Biomos, Zurich

18. Berendsen HJC, Postma JPM, van Gunsteren WF, Hermans J (1981) Interaction models for water in relation to protein hydration. In: Pullman B (ed) Intermolecular forces. Reidel, Dordrecht, pp 331–342
19. Hess B, Bekker H, Fraaije J, Berendsen HJC (1997) J Comp Chem 18:1463–1472
20. Miyamoto S, Kollman PA (1992) J Comp Chem 13:952–962
21. Scott EE, White MA, He YA, Johnson EF, Stout CD, Halpert JR (2004) J Biol Chem 279:27294–27301
22. Wester MR, Johnson EF, Marques-Soares C, Dansette PM, Mansuy D, Stout CD (2003) Biochemistry 42:6370–6379
23. Williams PA, Cosme J, Ward A, Angove HC, Matak Vinkovic D, Jhoti H (2003) Nature 424:464–468
24. Otyepka M, Skopalík J, Anzenbacherová E, Anzenbacher P (2007) Biochim Biophys Acta 1770:376–389
25. Poulos TL (2003) Proc Natl Acad Sci USA 23:13121–13122
26. Roussel F, Khan KK, Halpert JR (2000) Arch Biochem Biophys 374:269–278
27. Park H, Lee S, Suh J (2005) J Am Chem Soc 127:13634–13642
28. Li W, Liu H, Luo X, Zhu W, Tang Y, Halpert JR, Jiang H (2007) Drug Metab Dispos 35:689–696
29. Scott EE, He YQ, Halpert JR (2002) Chem Res Toxicol 15:1407–1413
30. Li W, Liu H, Scott EE, Grater F, Halpert JR, Luo X, Shen J, Jiang H (2005) Drug Metab Dispos 33:910–919
31. Podust LM, Poulos TL, Waterman MR (2001) Proc Natl Acad Sci USA 98:3068–3073
32. Raag R, Li H, Jones BC, Poulos TL (1993) Biochemistry 32:4571–4578
33. Li H, Poulos TL (1997) Nat Struct Biol 4:140–146